AIAA JOURNAL
Vol. 42, No. 8, August 2004

Technical Notes

TECHNICAL NOTES are short manuscripts describing new developments or important results of a preliminary nature. These Notes cannot exceed six manuscript pages and three figures; a page of text may be substituted for a figure and vice versa. After informal review by the editors, they may be published within a few months of the date of receipt. Style requirements are the same as for regular contributions (see inside back cover).

Modified Bang–Bang Vibration Control Applied to Adaptive Thin-Walled Beam Cantilevers

Sungsoo Na*
Korea University, Seoul 136-701, Republic of Korea
Liviu Librescu†
Virginia Polytechnic Institute and State University, Blacksburg, Virginia 24061
and
Jae-Hong Shim‡
Korea Polytechnic University, Jungwang-dong 429-793, Republic of Korea

Nomenclature

a_{33}, a_{55}	=	transverse bending and transverse shear stiffnesses, respectively
b_1, b_2	=	inertia coefficients
b, c	=	beam height and chord, respectively
E, G'	=	Young's modulus and transverse shear modulus, respectively
$\hat{J}$	=	generalized energy of the system
L	=	beam span
$\hat{M}_x$	=	piezoelectrically induced bending moment
$\boldsymbol{M}, \boldsymbol{K}$	=	mass and stiffness matrices, respectively
p_y	=	transversal load
$\boldsymbol{Q}$	=	generalized vector of time-dependent external excitations
$\boldsymbol{q}_v, \boldsymbol{q}_s$	=	vectors of generalized coordinates
t	=	time
$V_{\max}$	=	maximum allowed voltage
$\tilde{V}$	=	normalized transverse displacement
$\boldsymbol{V}, \boldsymbol{S}$	=	vectors of trial functions
Z^a	=	extension of the piezopatch along the beam span
δ_P, δ_S	=	tracers that take the value 1 or 0
θ_x	=	rotation of the normal about the x axis

I. Introduction

THE problem of the active vibration control of thin-walled beam cantilevers exposed to an external blast is addressed. The study is based on the implementation of smart materials technology in conjunction with piezoelectric strain actuation and on the requirement that the applied time-dependent electrical voltage be bounded. Both piezoactuators spread over the entire beam span and a piezopatch located along the beam span are considered. In both cases, out-of-phase activation is implemented.

As a result, in the case of the piezoactuators spread over the entire span, a piezoelectric bending moment is generated at the beam tip, whereas in the case of a piezopatch, bending moments are induced at the extremities of the patch. In the former case the induced bending moment appears in the boundary conditions at the beam tip, whereas in the latter, it appears in the governing equations.[1]

The control strategy applied in this study concerns the minimization of the dynamic response of the beam subject to a constraint on the input voltage applied to the piezoactuators. It was found[2] that a constraint voltage reduces the dynamic response for a certain time interval, after which the response starts to increase. At the end of this time duration, either the sign of the voltage is reversed or the voltage is set equal to zero for a certain time interval, at the end of which the voltage is again set to a positive or negative value to continue reducing the dynamic response.

This implies that the voltage sign should be changed at the end of each time interval, or should become zero, the switchover time being determined by the requirement of achieving the fastest decrease of the dynamic response.

II. Basic Assumptions and Governing Equations

In this study the feedback vibration control of thin-walled beam cantilevers exposed to an external blast is addressed. The beam model features 1) transverse isotropy of constituent material layers, the surface of isotropy being parallel to the beam reference surface, and 2) transverse shear effects.

The points on the beam cross sections are identified by the global coordinates (x, y, z), where z is the spanwise coordinate and (x, y) are the cross-sectional ones. See the paper by Na and Librescu.[1] With the previously stated assumptions, exact decoupling of transverse (flapping) and lateral (lagging) twist and of longitudinal motions is featured. Here, we confine our attention to transverse bending only. Based on the previously mentioned assumptions, and using Hamilton's principle, the equations governing the transverse bending of thin-walled beams that are clamped at $z = 0$ and free at $z = L$, as obtained by Song and Librescu,[3] are

$$\delta v_0 : a_{55}(v_0' + \theta_x)' + p_y(z,t) = b_1 \ddot{v}_0 \tag{1a}$$

$$\delta\theta_x : a_{33}\theta_x' - a_{55}(v_0' + \theta_x) - \delta_P \hat{M}_x' = \underline{b_2 \ddot{\theta}_x} \tag{1b}$$

and the boundary conditions

$$v_0 = 0 \tag{2a}$$

$$\theta_x = 0 \tag{2b}$$

at $z = 0$ and

$$v_0' + \theta_x = 0 \tag{2c}$$

$$a_{33}\theta_x' = \delta_S \hat{M}_x \tag{2d}$$

at $z = L$. Here $p_y(z,t)$ denotes the distributed transverse load, and the underscored term in Eq. (1b) corresponds to the rotatory inertia effect, whereas the primes denote the derivatives with respect to

Received 20 February 2003; revision received 6 February 2004; accepted for publication 8 February 2004.

*Associate Professor, Department of Mechanical Engineering. Member AIAA.
†Professor, Engineering Science and Mechanics.
‡Associate Professor, Department of Control and Measurement Engineering.

the spanwise z coordinate. In addition, $\hat{M}_x$ is the piezoelectrically induced bending moment, and in this connection, δ_S and δ_P are two tracers that identify the cases of the piezoactuators distributed over the entire beam span or in the form of a patch, respectively. In the former case, the piezoelectrically induced bending moment appears at the beam tip only, implying that $\delta_S = 1$, $\delta_P = 0$, and in the latter, it appears only in the governing equations, implying that $\delta_S = 0$, $\delta_P = 1$. In addition, a_{33} and a_{55} define the bending and transverse shear stiffness quantities, respectively, whereas b_1 and b_2 denote the inertia coefficients.

The stiffness quantities a_{ij} and the inertia terms b_i can be cast in a unified form for both piezoactuator distributions as $a_{ij} = \bar{a}_{ij} + \delta_P \hat{a}_{ij} + \delta_S \hat{\hat{a}}_{ij}$, $b_i = \bar{b}_i + \delta_P \hat{b}_i + \delta_S \hat{\hat{b}}_i$, where the terms marked by an overbar or by circumflex signs are associated with the host structure and with the piezoactuators, respectively. Their expressions are supplied in different contexts in the paper by Na and Librescu.[1]

III. Piezoactuator Distribution

It is assumed that the host structure and the actuators consist of m layers and of l piezoelectric material layers, respectively, both of these featuring transversally isotropic properties. As a result, for piezoactuators the n axis of the structure constitutes an axis of rotary symmetry that coincides with the direction of polarization (thickness polarization). One assumes that the piezoactuators are bonded to the top and bottom faces of the beam and that they are either spread over its entire span or in the form of a patch located along the beam span.

In such conditions, a bending moment is generated at the beam tip in response to an applied electrical field E_3. In this case, vibrational feedback control is accomplished via boundary moment control.

In contrast to this case, that is, when a piezoelectric patch is involved, the bending moment $\hat{M}_x \equiv \hat{M}_x(z, t)$ appears solely in the governing equations. In this case, the piezoelectrically induced bending moment is expressed as

$$\hat{M}_x(z, t) = \boldsymbol{C} V(t)[Y(z - z_1) - Y(z - z_2)] \tag{3}$$

where $\boldsymbol{C}$ is a constant dependent on the mechanical and geometrical properties of the piezoactuator and host structure, $V(t)$ is the applied input voltage (out-of-phase actuation), and z_1 and z_2 are the piezoend points, whereas $Y(z)$ is the Heaviside distribution.

Needless to say, $\hat{M}_x(z, t)$ appears to be a function of the geometrical and mechanical properties of the piezoactuators and of the applied input voltage. The expression of the piezoelectrically induced moment occurring in each of these cases has been provided in the paper by Librescu et al.[4] and will not be repeated here.

IV. Discretized Equations and Bang–Bang Control

To discretize the boundary-value problem, $v_0(z, t)$ and $\theta_x(z, t)$ are represented as

$$v_0(z, t) = \boldsymbol{V}^T(z)\boldsymbol{q}_v(t), \qquad \theta_x(z, t) = \boldsymbol{S}^T(z)\boldsymbol{q}_s(t) \tag{4}$$

where $\boldsymbol{V}(z)$ and $\boldsymbol{S}(z)$ are the vectors of trial functions that should fulfill all of the kinematic boundary conditions and are assumed to be known; $\boldsymbol{q}_v(t)$ and $\boldsymbol{q}_s(t)$ are vectors of generalized coordinates, whereas the superscript T denotes the transpose operation.

The representations of displacement measures are used directly in Hamilton's principle, on the basis of which Eqs. (1) and (2) were obtained. In this context, the solution methodology that was used is referred to as the extended Galerkin method. For more details see the paper by Librescu et al.[5]

As a result of its application, an equation expressed in matrix form is obtained:

$$\boldsymbol{M}\ddot{\boldsymbol{q}} + \boldsymbol{K}\boldsymbol{q} = \boldsymbol{Q} - \boldsymbol{F}\boldsymbol{u} \tag{5}$$

Here $\boldsymbol{q}[\equiv [\boldsymbol{q}_v^T, \boldsymbol{q}_s^T]^T]$ is a $2N \times 1$ column matrix whose elements are $q_i(t)$, and $\boldsymbol{M}$ and $\boldsymbol{K}$ denote the mass and stiffness matrices, respectively, of the structure considered in its entirety (i.e., of host and piezoactuators), which are $2N \times 2N$ square matrices. Their expressions are not displayed here.

In addition, $\boldsymbol{u}$ is the vector of the control input, and $\boldsymbol{Q}(\equiv \boldsymbol{Q}(t))$ is the generalized vector of time-dependent external excitations, given by

$$\boldsymbol{Q} = \int_0^L p_y(z, t)\boldsymbol{V}^T(z)\,\mathrm{d}z$$

The control strategy to be applied involves the minimization of the dynamic response of the beam, subject to a constraint on the maximum input voltage that can be applied to the piezoactuators. The minimization is achieved by applying the voltage in such a manner that the dynamic response of the structure is reduced with time. As shown by Bruch et al.,[2] a constraint voltage reduces the dynamic response for a certain time duration, after which the response starts to increase. At the end of this duration, either the sign of the voltage is reversed or the voltage is set equal to zero for a certain time interval. At the end of that time interval the electrical voltage is again set to positive or negative to continue reducing the dynamic response. In this context, the following optimal control problem is formulated:

Find the scalar control function $u = u(t)$ that minimizes the performance index

$$J = \int_0^{t_f} [\boldsymbol{X}^T \boldsymbol{Z} \boldsymbol{X}]\,\mathrm{d}t \tag{6a}$$

subject to the constraint

$$|u(t)| \le V_{\max} (0 \le t \le t_f) \tag{6b}$$

In Eq. (6a), $\boldsymbol{Z}$ is a positive definite weighting matrix, whereas in Eq. (6b), $V_{\max}$ is the maximum allowed voltage and $\boldsymbol{X}(t = 0) \equiv \boldsymbol{X}(0) = \boldsymbol{X}_0$, $\boldsymbol{X}(t_f) = 0$, where t_f is the free time.

The state-weighting matrix $\boldsymbol{Z}$ was chosen in the form

$$\boldsymbol{Z} = \begin{bmatrix} \boldsymbol{K} & \boldsymbol{0} \\ \boldsymbol{0} & \boldsymbol{M} \end{bmatrix} \tag{7}$$

so that the cost functional represents the sum of the system kinetic and strain energies. As a result,

$$J = \int_0^{t_f} \hat{J}\,\mathrm{d}t$$

where $\hat{J} \equiv \dot{\boldsymbol{q}}^T \boldsymbol{M} \dot{\boldsymbol{q}} + \boldsymbol{q}^T \boldsymbol{K} \boldsymbol{q}$ defines the generalized energy of the system.

In this context, the control methodology reduces to optimal bang–bang type control, where its approach is achieved in conjunction with Pontryagin's minimum principle.

To eliminate the inherent shortcomings arising from its application,[6] a modified bang–bang control strategy that parallels the one advanced by Bruch et al.[2] is used here, namely

$$u(t) = -V_{\max}\,\mathrm{sgn}(\mathcal{E}(t_i)) \tag{8a}$$

where

$$\mathcal{E}(t_i) = \hat{J}(t + \Delta t; V_i) - \hat{J}(t; V_i) \tag{8b}$$

for $t_i \le t \le t_{i+1}$, Δt being a specified time interval, $\mathrm{sgn}(\cdot)$ denoting the signum distribution, that is, $+1$ or -1, depending on whether the argument is positive or negative, and V_i being the input voltage at time $t = t_i$. The control law expressed by Eqs. (8) is referred to as suboptimal bang–bang control. The voltage $u(t_i)$ and the switching time t_i are determined so that the performance index (6a) is minimized as time unfolds, while also fulfilling the constraint equation (6b).

V. Numerical Simulations

The displayed numerical results are restricted to the case of a thin-walled single layer beam of symmetric biconvex cross-section profile.[1] The dynamic loads used in the numerical simulations correspond to explosive and step pulses. These are represented in the inset of each figure and are assumed to be of moderate intensity

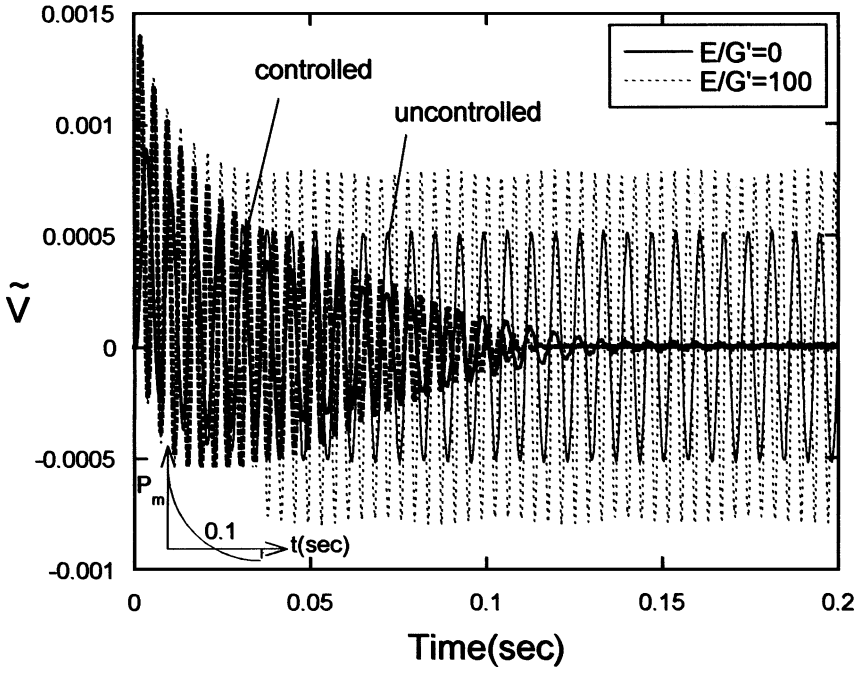

Fig. 1 Implications of transverse shear flexibility of the host beam for normalized deflection time history of the beam tip when it is subjected to a blast pulse [$a'/t_p = 80$; $t_p = 0.1$ s; $Z^a = (0.2–0.1)L$].

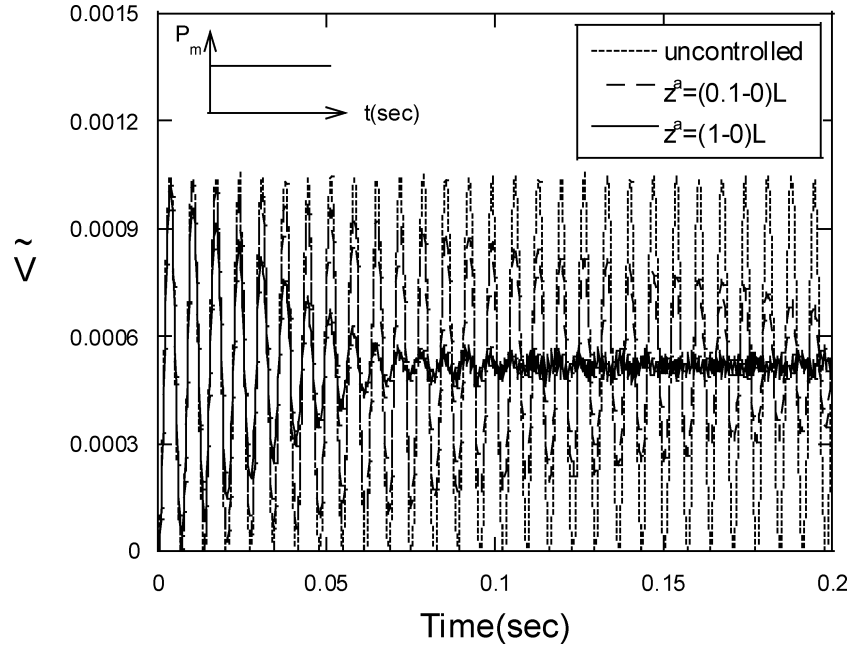

Fig. 2 Implications of the size of the piezoactuator patch for the deflection time history of the beam tip exposed to a step pulse ($E/G' = 0$).

in order not to damage the structure. The host structure is considered to be a transversely isotropic material characterized by the Young's modulus E on the surface of isotropy (coinciding with the beam midsurface) and the transverse shear modulus G' in the planes normal to the isotropy surface. The piezopatch is manufactured from lead-zirconate-titanate-4 (PZT-4) piezoceramic. For its properties and location see Refs. 1 and 4, respectively. Throughout these results, unless otherwise specified, the amplitude of the time-dependent load, $P_m = 50$ lb/L (222 N/L), the aspect ratio of the beam is $AR(\equiv 2L/c) = 6$ and $V_{\max} = 300$ Vs. In addition, the mass density of the material of the host structure considered in this study is $\rho = 0.143 \times 10^{-3}$ lb $\cdot$ s^2/in.^{4} (1.5×10^{-5} N $\cdot$ s^2/cm^4), the patch data are $S_a = 3.5$ in. (0.089 m), and $t_a = 0.00787$ in. (0.0002 m), whereas for the host structure the data are $c = 10$ in. (0.254 m), $b = 2.68$ in. (0.06807 m), and $h = 0.4$ in. (0.01016 m).

In Fig. 1 is depicted the time history of the normalized deflection $\tilde{V}(\equiv V(L)/L)$ of the beam tip cross section to an explosive blast, whose negative phase is included. Both transversely shearable ($E/G' = 100$) and unshearable ($E/G' = 0$) beams are considered. The results reveal that for the uncontrolled beam, the unshearable beam model provides an underestimate of the deflection. However, for the controlled beam, the differences of the predictions provided by the two models become marginal.

In Fig. 2 is displayed the time history of the normalized deflection of the beam tip subjected to a step pulse, for the cases 1) of the control achieved when there is a piezoactuator patch located along the beam span between $\eta_1 = 0$ and $\eta_2 = 0.1$ and 2) when the piezoactuator is spread over the entire beam span, that is, between $\eta_1 = 0$ and $\eta_2 = 1$. Here $\eta = z/L$ denotes the dimensionless spanwise coordinate. The supplied results reveal that in the case of the piezoactuators spread

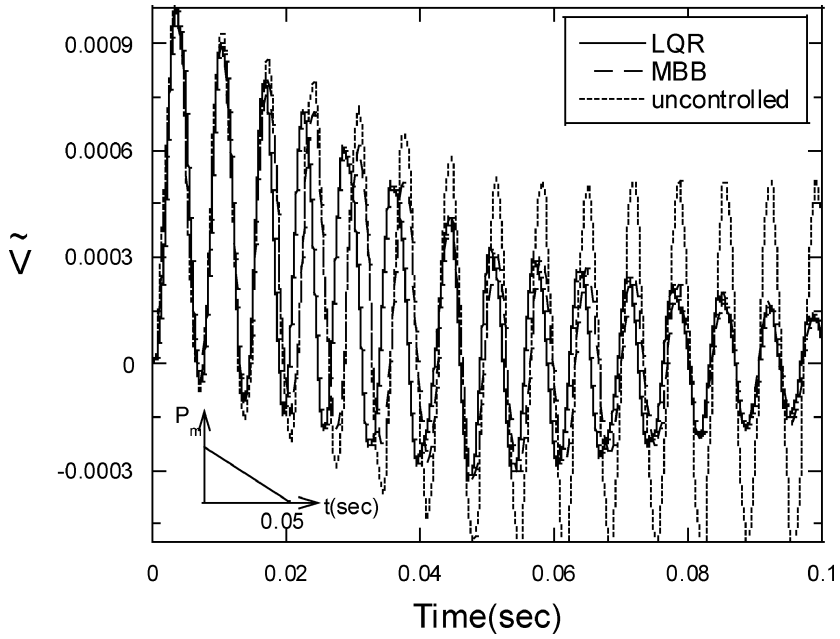

Fig. 3 Comparison of the results from the actual bang–bang and optimal LQR control methodologies for the deflection time history of the beam tip exposed to a blast pulse [$Z^a = (0.3–0.1)L$].

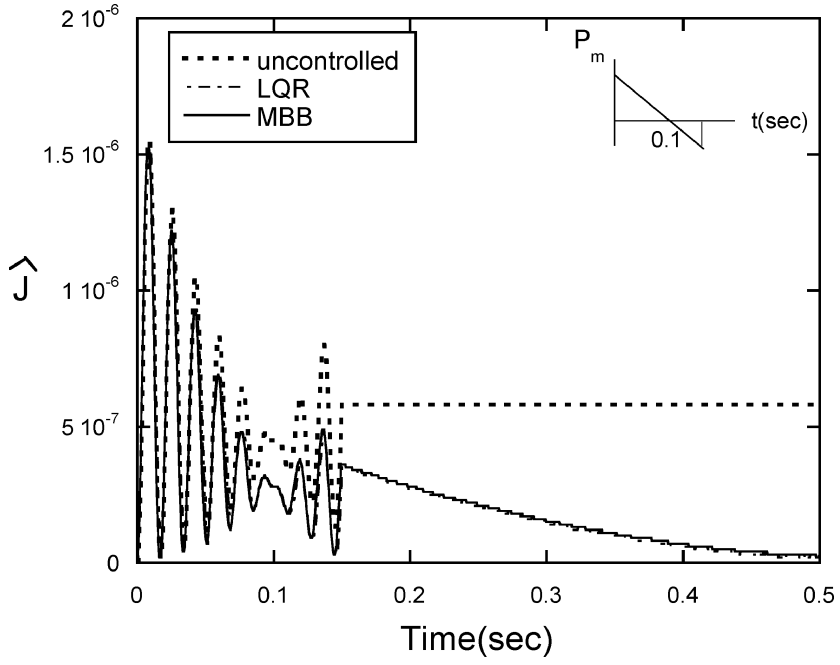

Fig. 4 Comparison of the performance of the MBB and LQR in controlling the total energy timehistory of the beam impacted by a sonic boom [$r = 1.5$; $t_p = 0.1$ s, $Z^a = (0.3–0.1)\ L$; $E/G' = 0$]. The uncontrolled response is also displayed.

over the entire span the control appears more effective than in the case of the piezopatch actuator. However, having in view the weight penalty introduced in case 2, one can conclude that the former option is preferable to the latter.

In Fig. 3, predictions based on modified bang–bang (MBB) and standard linear quadratic regulator (LQR) control methodologies are compared. The beam is exposed to a blast pulse. The results reveal that the bang–bang control is more efficient than the LQR in damping out the oscillations. In a different context, these findings are in excellent agreement with those reported in Ref. 6.

Finally, in Fig. 4, the time history of the total energy $\hat{J}$ for the uncontrolled and controlled beams is displayed. In the latter context, the LQR and MBB results are compared. The system is impacted by a sonic-boom pulse. The results reveal that both control methodologies are extremely efficient in reducing to zero the total energy as the time unfolds. The results also reveal that for the unactivated system, in the free motion regime, due to the absence of structural damping, the total energy remains uniform in time.

VI. Conclusions

A modified bang–bang control strategy was applied to the dynamic response control of thin-walled beam cantilevers exposed to a blast. The implications of a number of effects, which include those related to the size and location of piezoactuators and the type of pressure pulse, have been discussed, comparisons with predictions obtained via the application of the LQR control methodology have been presented, and pertinent conclusions have been outlined. Although applied in a rather simplified structural context, this control methodology is likely to provide excellent results for more complex structural configurations, as well.

Acknowledgment

Sungsoo Na acknowledges the support by the Basic Research Program of the Korea Science and Engineering Foundation, Grant R01-2002-000-00129-0.

References

[1]Na, S. S., and Librescu, L., "Optimal Vibration Control of a Thin-Walled Anisotropic Cantilevers Exposed to Blast Loadings," *Journal of Guidance, Control, and Dynamics*, Vol. 23, No. 3, 2000, pp. 491–500.

[2]Bruch, J. C., Jr., Sloss, J. M., Adali, S., and Sadek, I. S., "Modified Bang–Bang Piezoelectric Control of Vibrating Beams," *Smart Materials and Structures*, Vol. 8, 1999, pp. 647–653.

[3]Song, O., and Librescu, L., "Bending Vibration of Cantilevered Thin-Walled Beams Subjected to Time-Dependent External Excitations," *Journal of the Acoustical Society of America*, Vol. 98, No. 1, 1995, pp. 313–319.

[4]Librescu, L, Song, O., and Rogers, C. A., "Adaptive Vibrational Behavior of Cantilevered Structures Modeled as Composite Thin-Walled Beams," *International Journal of Engineering Science*, Vol. 31, No. 5, 1993, pp. 775–792.

[5]Librescu, L., Meirovitch, L., and Na, S. S., "Control of Cantilevers Vibration via Structural Tailoring and Adaptive Materials," *AIAA Journal*, Vol. 35, No. 8, 1997, pp. 1309–1315.

[6]Wu, Z., and Soong, T. T., "Modified Bang–Bang Control Law for Structural Control Implementations," *Journal of Engineering Mechanics*, Vol. 122, No. 8, 1996, pp. 771–777.

C. Pierre
Associate Editor

Experimental Verification of the Mach-Number Field in a Supersonic Ludwieg Tube

M. Y. El-Naggar,* J. T. Klamo,* M.-H. Tan,†
and H. G. Hornung‡
California Institute of Technology,
Pasadena, California 91125

I. Introduction

A NEW supersonic Ludwieg tube (LT) was completed at the California Institute of Technology (Caltech) in 2000. A LT, first proposed by Hubert Ludwieg in 1955 in response to a competition (see also Ludwieg et al.[1]), is a blowdown wind tunnel in which the high-pressure reservoir is a long tube. The flow is started by rupturing a diaphragm. The advantage of the long high-pressure reservoir is that, during the time it takes for the expansion wave generated by diaphragm rupture to propagate to the far end of the tube and for its reflection to come back to the diaphragm station, a perfectly uniform reservoir devoid of wave reflections is available to drive a supersonic nozzle. In the Caltech LT, the diaphragm station is located downstream of the nozzle to permit a smooth transition from the tube to the nozzle. Also, the boundary layer developing in the long tube is sucked off through an annular throat just upstream of the nozzle entrance, so that a clean flow is generated. The 300-mm-diam tube is 17 m long, the nozzle was designed for a Mach number of 2.3 by J. J. Korte of NASA Langley Research Center, and the test section cross section is 200 × 200 mm. The useful test time is 75 ms. The aim of the present work was to determine the detailed Mach-number and flow-direction fields by using the method of visualization of Mach waves that was first used by Meyer.[2]

II. Mach-Wave Method

In a steady supersonic flow, disturbances that cause flow deflections generate shock or expansion waves. If the disturbance is infinitesimally small, the wave generated makes an angle μ to the flow that is given by

$$\sin\mu = 1/M \tag{1}$$

where M is the local Mach number. If two disturbances generate waves that intersect at a point in the flowfield, the local streamline direction bisects the angle made by the two waves, and the latter is therefore 2μ. If sufficiently weak waves can be generated in an experimental flow so that their intersection angle approximates this value closely, visualization of the waves can be used to determine both the local flow direction and the Mach number.

The method is particularly useful in plane flow because weak plane waves are very easily detectable by line-of-sight integrating methods such as schlieren or shadowgraph techniques. The two-dimensional nozzle of the LT is thus an ideal candidate for the method. The sensitivity of the method can be obtained by differentiating Eq. (1):

$$\frac{\mathrm{d}\mu}{\mathrm{d}M} = -\frac{1}{M\sqrt{M^2-1}} \tag{2}$$

showing that it is infinitely sensitive at $M = 1$ and has zero sensitivity at $M = \infty$. At $M = 2.3$ a change of Mach number by 0.01 causes a change of μ of 0.12 deg. The accuracy of the method depends on how weak detectable waves can be made and how accurately the wave angles can be measured. In the Mach-number range of the flow studied here ($\leq$2.3) the numbers look promising.

To get a rough idea of how small the strength of the wave has to be for the wave angle to be close enough to μ, an inviscid computation of supersonic flow over a disturbance such as a strip of adhesive tape was made. The result of this computation is shown in Fig. 1. The calculation shows the characteristic divergence of the leading and trailing shock waves. According to weak shock theory,[3] these two shocks lie on a curve of the form

$$y = \left(x\Big/\sqrt{M^2-1}\right) \pm a\sqrt{x} \tag{3}$$

where a is a constant that depends on the obstacle shape. Thus, these two shocks give a very good measure of the Mach angle only in the very far field.In the physical flow, the disturbances are generated by strips of adhesive tape stuck to the top and bottom walls of the nozzle. They are only 0.1 mm thick and are therefore embedded in the nozzle–wall boundary layer and see a flow at a Mach number much smaller than 2.3, so that the waves they generate are much weaker than those in the inviscid computation. This is the reason for our choice of the wedge-shaped leading edge in the computation. Two other features of the flow are the expansion fans from the leading and trailing shoulders of the obstacle. Two straight lines are drawn in the figure at the Mach angle, approximately from the two shoulders. As may be seen, the leading characteristic from the trailing shoulder is almost immediately parallel to the line.

For the computation, the software system Amrita, constructed by J. Quirk,[4] was used. Amrita is a system that automates and packages computational tasks in such a way that the packages can be combined (dynamically linked) according to instructions written in a high-level scripting language. The present application uses features of Amrita that include the automatic construction of an Euler solver, automatic adaptive mesh refinement according to simply chosen criteria, and scripting-language-driven computation and postprocessing of the results. The Euler solver generated for the present computation was an operator-split scheme with HLLE flux and kappa-MUSCL reconstruction. The computation is made with a 90 × 60

Received 27 June 2003; accepted for publication 5 February 2004.

*Graduate Student, Mechanical Engineering, MC 104-44, 1200 E. California Boulevard.

†Graduate Student, Graduate Aeronautical Laboratories, 1200 E. California Boulevard.

‡C. L. "Kelly" Johnson Professor of Aeronautics, Graduate Aeronautical Laboratories, 1200 E. California Boulevard. Lifetime Fellow AIAA.